Nat. Hazards Earth Syst. Sci. Discuss., https://doi.org/10.5194/nhess-2018-6
Manuscript under review for journal Nat. Hazards Earth Syst. Sci.
Discussion started: 24 January 2018


Natural Hazards and Earth System Sciences
Open Access
Discussions

# Forecasting post-failure landslide mobility using a SPH model and data from ring shear strength tests: A case study

Miao Yu[1], Yu Huang[2,3]*, Wenbin Deng[2], Hualin Cheng[2]

[1] Faculty of Engineering, China University of Geosciences, Wuhan, Hubei 430074, China

[2] Department of Geotechnical Engineering, College of Civil Engineering, Tongji University, Shanghai 200092, China

[3] Key Laboratory of Geotechnical and Underground Engineering of the Ministry of Education, Tongji University, Shanghai 200092, China

* Corresponding author: Yu Huang (Tel.: +86-21-6598-2384; Fax: +86-21-6598-5210. E-mail: yhuang@tongji.edu.cn)

**Abstract** Flowlike landslides, such as flowslides and debris avalanches, have caused serious infrastructure damage and casualties for centuries. Effective numerical simulation incorporating accurate soil mechanical parameters is essential for predicting post-failure landslide mobility. In this study, smoothed particle hydrodynamics (SPH) incorporating soil ring shear test results was used to forecast the long-runout mobility for a landslide on an unstable slope in China. First, a series of ring shear tests under different axial stresses and shear velocities were conducted to evaluate the residual shear strength of slip zones after extensive shear deformation. Based on the ring shear test results, SPH modeling was conducted to predict the post-failure mobility of a previously identified unstable slope. The results indicate that

Nat. Hazards Earth Syst. Sci. Discuss., https://doi.org/10.5194/nhess-2018-6
Manuscript under review for journal Nat. Hazards Earth Syst. Sci.
Discussion started: 24 January 2018


the landslide would cut a fire road on the slope after 12 s and cover an expressway at the foot of that slope after 36 s. In the model, the landslide would finally stop sliding about 25 m beyond the foot of the slope after 120 s. This study shows that combining the SPH method with ring shear test results to forecast landslide mobility can provide basic information for landside disaster mitigation.

**Keywords:** Landslide hazard; Post-failure mobility; Ring shear tests; Smoothed particle hydrodynamics (SPH); Residual strength

## 1. Introduction

Flowlike landslides triggered by intense earthquakes or rainfall, such as debris and rock avalanches, have caused serious infrastructure damage and casualties for centuries (Okada et al. 2007; Wang et al. 2005). This kind of landslide is commonly high-speed and has a long runout distance. For example, a large landslide in southern Italy in February, 2010, had a runout distance of 1.2 km and necessitated the evacuation of nearly 2,300 people. This landslide was triggered by heavy and prolonged rainfall between August 2009 and February 2010 (Gattinoni et al. 2012). The 2009 Shiaolin landslide in Taiwan, induced by a cumulative rainfall of nearly 1700 mm from Typhoon Morakot, buried Shiaolin Village and resulted in more than 400 people dead and missing (Tsou et al. 2011). Numerical simulations that incorporate accurate soil mechanical parameters are a powerful tool for simulating landslide runout distances; these simulations can provide fundamental reference information for landside disaster mitigation (Yerro et al. 2016; Žic et al. 2015).

Nat. Hazards Earth Syst. Sci. Discuss., https://doi.org/10.5194/nhess-2018-6
Manuscript under review for journal Nat. Hazards Earth Syst. Sci.
Discussion started: 24 January 2018


The main numerical methods for simulating landslides are the discrete element methods and the continuum methods (Lu et al. 2014; Wu et al. 2017). Using a discrete element method, such as the distinct element method (DEM) or discontinuous deformation analysis (DDA), the nonphysical parameters cannot be determined exactly (Huang et al. 2014). However, continuum methods based on grids, like the finite element method (FEM) and the finite difference method (FDM), have the shortcomings of grid distortion and low accuracy for the numerical analysis of a landslide with a long runout. Recently, a new numerical method has been used to overcome these limitations, namely the smoothed particle hydrodynamics method (SPH) (Bui et al. 2008). This method is in the framework of continuum methods. SPH is a pure Lagrangian, meshless hydrodynamics method and it is capable of simulating flow deformation, free surfaces, and deformation boundaries (Liu and Liu 2003). Several studies have demonstrated the efficiency of the SPH method for the large deformation analysis post landslide. Huang et al (2014) provided a general view of SPH applications for solving large deformation and failure problems such as dam breaks, slope failure, and soil liquefaction flow. Pastor et al (2009) applied a depth-integrated, coupled SPH model successfully to simulate catastrophic flow-like landslides that occurred in southern Italy in 1998. Cascini et al (2014) proposed a SPH model to represent two actual flow-type events accurately. Cuomo et al (2016) used SPH to simulate flow-like landslides (debris flows and debris avalanches) and discussed the influence of bed entrainment on landslide propagation. Hu et al (2015) conducted two- and three-dimensional SPH numerical simulation of flow-like landslides triggered by the 2008 Wenchuan earthquake in China and proposed that the SPH method is well-suited for modeling free surfaces, moving interfaces, and extensive deformation.

Study into the residual shear strength property of slip zones under large shear deformation is essential to landslide long-runout mechanism explanation (Tika and Hutchinson 1999; Wen et al. 2007). Because the physical sample displacement using conventional laboratory shear tests, like direct shear tests and triaxial shear tests, is limited to about 10 mm (Okada et al. 2007; Casagli et al. 2006; Van Asch et al 2007), the shear behavior for large shear displacements cannot be assessed by these methods (Dai et al. 2016). Ring shear tests, which can impart extremely large shear strains, may be the ideal laboratory tool for extensive shear deformation testing (Okada et al. 2007; ASTM Standard D7608-10, 2010). Several studies have applied ring shear tests to study the residual shear strength of soils (Fukuoka et al, 2007; Hoyos et al. 2014; Li et al. 2013; Wang et al. 2005). For example, Fukuoka et al (2007) applied a newly developed ring shear test to study shear zone development during large displacements. That study pointed out that a ring shear test is the most appropriate test for studying long-travel landslides. Kimura et al (2014) studied the effect of the shearing rate on the residual strength of landslide soils using ring shear tests. Zhang et al (2011) used ring shear tests to study the transform mechanism of the slide-debris flow under large

Nat. Hazards Earth Syst. Sci. Discuss., https://doi.org/10.5194/nhess-2018-6
Manuscript under review for journal Nat. Hazards Earth Syst. Sci.
Discussion started: 24 January 2018

Natural Hazards and Earth System Sciences
Open Access
Discussions

deformation. Li et al (2017) explored the residual strength of silty sand under different degrees of over consolidations and different shear rates using ring shear tests.

This study presents an effective numerical simulation method, namely SPH, that incorporates accurate soil mechanical parameters derived from ring shear tests. The aim is to predict the downslope flow after slope failure of a previously identified unstable slope and thereby provide basic information for landside disaster mitigation. First, this paper describes the geomorphological and geological setting, hydrogeology and rainfall, and triggering factors of the landslide examined for this case study. These descriptions are based on detailed fieldwork. Next, a series of ring shear tests under several different normal stresses and shear rates were performed to identify the shear strength of the landslide soil. Finally, a SPH-based numerical simulation of the landslide was run to predict the extent of the landslide and track the slide velocity at different times.

## 2. A case study – the Dafushan landslide

### *2.1 Geomorphological and geological setting*

The Dafushan landslide, located in the Panyu District, Guangzhou City, South China, was selected for this case study (Fig. 1(a)). The slope is primarily composed of Cretaceous silty mudstone, conglomerate, and sandstone overlain by Quaternary silty clay (Yu et al. 2017) (Fig. 1(b)). The landslide is creeping from the northeast to the southwest covering an area of about 70 m × 40 m (Fig. 1(c)). The height difference between the toe and the crown is approximately 20 m with an average gradient of 25°.

Nat. Hazards Earth Syst. Sci. Discuss., https://doi.org/10.5194/nhess-2018-6
Manuscript under review for journal Nat. Hazards Earth Syst. Sci.
Discussion started: 24 January 2018


The Dongxin expressway and a 50 t, high-voltage power line tower are located at the toe and top of the slope, respectively. In addition, there is a fire response service road that runs along the slope that is affected by the slide (Fig. 1(d)).

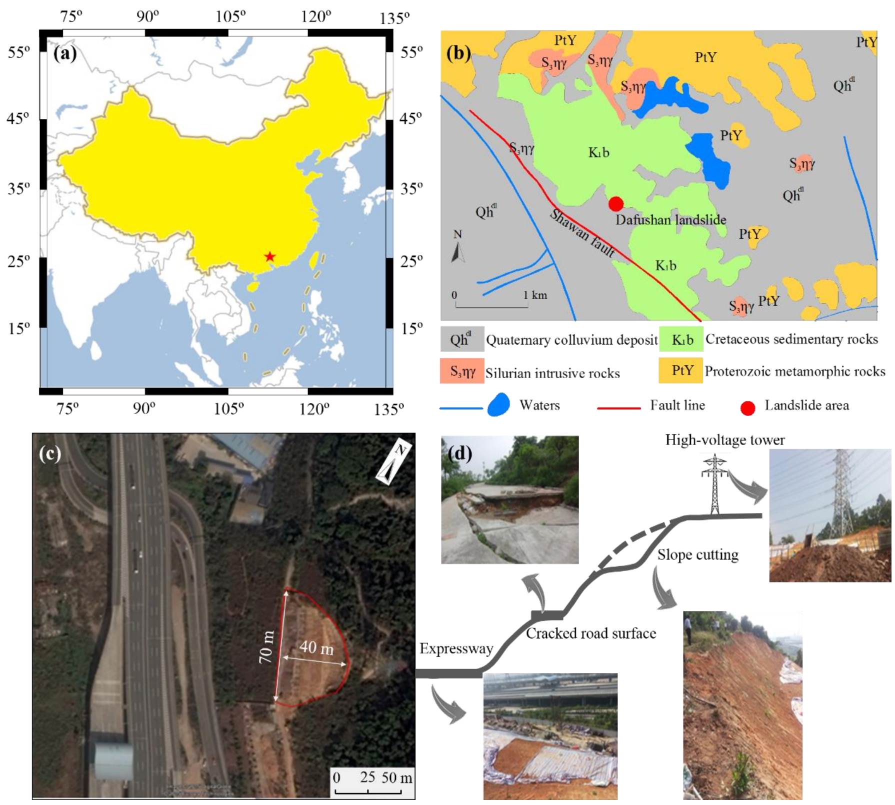


**Fig. 1.** Overview of the Dafushan landslide. (a) Landslide location; (b) Geomorphologic and geologic map of the landslide area; (c) Aerial view of the unstable (potential landslide area (the area inside the red lines) (image from Google Earth®); (d) Engineering activities on the slope (reprinted from Yu et al. (2017) with permission of Springer).

*2.2 Landslide triggering factors*

Nat. Hazards Earth Syst. Sci. Discuss., https://doi.org/10.5194/nhess-2018-6
Manuscript under review for journal Nat. Hazards Earth Syst. Sci.
Discussion started: 24 January 2018


The ground was first found to be unstable in May 2013. This instability was manifested mainly by cracks in the ground surface and cracks in the round-the-mountain road. The road was built for fire response services in May 2011. The relevant departments repaired the damaged road immediately to guarantee the normal operation of the road. However, addition evidence of instability was found in the middle of August 2013 after a period of intense rainfall. The road was damaged again and the trees up the hill began to tilt. Based on preliminary field investigation, the main factors that triggered the landslide were deduced.

*(1) Hydrogeology and rainfall*

Rainfall is the main supply source of groundwater in the study area. The average annual rainfall is 1635.6 mm. Most of the rain falls between April and September; this rainfall accounts for 81% of the yearly precipitation. In the rainy season, the groundwater level rise significantly and reduces the shear strength of the soil. Combined with the rainfall flushing effect on the slope surface, the stability of the slope is decreased significantly.

*(2) Mechanical properties of landslide soil*

The shallow part of the landslide is mainly composed of silty clay (Fig. 2) and a strongly weathered mudstone soil with a low shear strength. These materials soften and disintegrate when wet, thus the slope is stable in the dry season but shows signs of instability in the rainy season.

Nat. Hazards Earth Syst. Sci. Discuss., https://doi.org/10.5194/nhess-2018-6
Manuscript under review for journal Nat. Hazards Earth Syst. Sci.
Discussion started: 24 January 2018


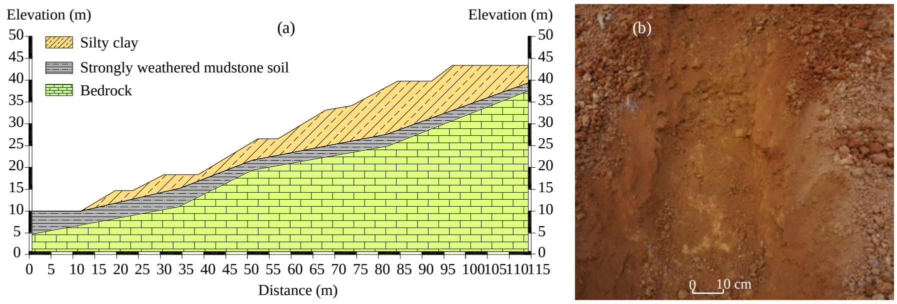


**Fig. 2.** Geology and soil at the Dafushan landslide. (a) Longitudinal geologic section of the unstable slope shown in Fig. 1(c). (b) Photograph of the silty clay landslide soil.

*(3) Human engineering activities*

Human engineering activities impaired the natural stability of the slope. Two examples: a) to build the fire service road, a cut was made in the slope; b) the heavy high-voltage power line tower increases the downward pressure on the slope (Fig. 1(d)).

## 3. Ring shear tests

A GCTS Residual Ring Shear Testing System (model SRS-150) produced by Geotechnical Consulting and Testing Systems (GCTS) in 2012 in the USA was used for the ring shear tests conducted for this study (Fig. 3). The SRS 150 is a fully automated electro-pneumatic and servo-controlled testing system used for determining the residual strength of continuously sheared soil. Shear torques of up to 820 Nm can be applied, consolidation stress can be up to 1000 kPa, and unlimited angular rotation is allowed (Dai et al. 2016; Hoyos et al. 2014). The unit is capable of applying shearing rates of 0.001 to 360 degrees per minute continuously with

Nat. Hazards Earth Syst. Sci. Discuss., https://doi.org/10.5194/nhess-2018-6
Manuscript under review for journal Nat. Hazards Earth Syst. Sci.
Discussion started: 24 January 2018


zero-backlash for replication of true in-situ strain rates during failure. (Hoyos et al. 2011).


**Fig. 3.** Photograph of the GCTS SR-150 Residual Ring Shear testing device and an image of the GCTS software interface.

A schematic illustration of a sample in the apparatus is shown in Fig. 4. For testing granular materials, the device accepts ring-shaped samples with a 150 mm outer diameter and a 100 mm inner diameter. The sample is sheared by rotating the upper half of the testing unit and keeping the lower half motionless. Two types of shearing modes, either a shear speed control mode or a shear torque control mode, can be chosen.

Nat. Hazards Earth Syst. Sci. Discuss., https://doi.org/10.5194/nhess-2018-6
Manuscript under review for journal Nat. Hazards Earth Syst. Sci.
Discussion started: 24 January 2018


Natural Hazards and Earth System Sciences
Open Access
Discussions

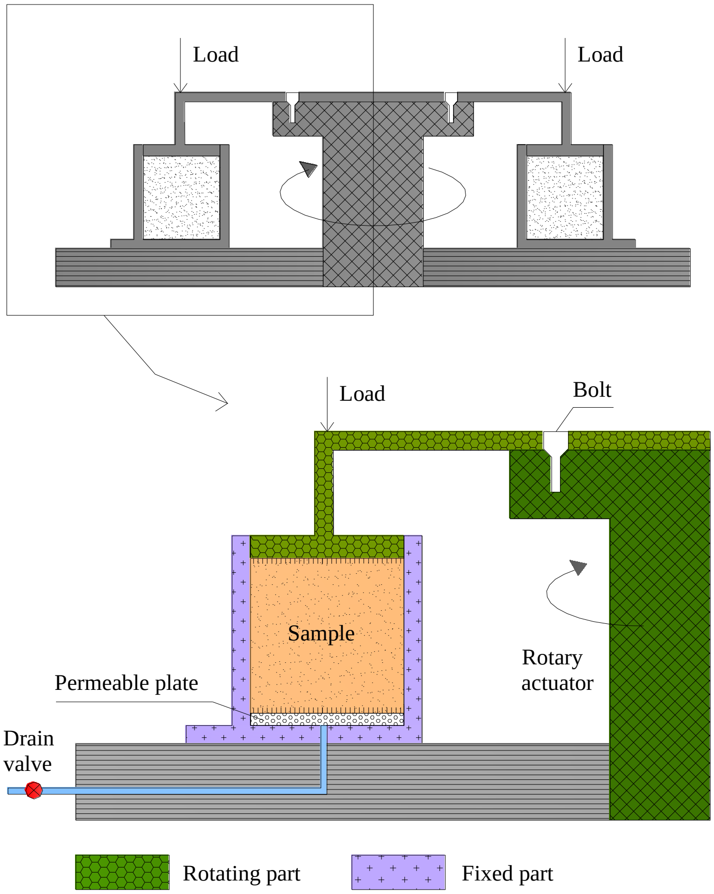


**Fig. 4.** Schematic cross sections of ring shear apparatus shown in Figure 3.

*3.1 Sample preparation and test procedures*

The samples studied were samples of the silty clay soil from the Dafushan landslide shown in Fig. 2(b). The soil's physical properties are listed in Table 1.

**Table 1** Physical properties of a soil from the Dafushan landslide.

| Density $\rho$ (g/cm$^3$) | Dry density $\rho_d$ (g/cm$^3$) | Water content $\omega$(%) | Liquid limit $\omega_L$ | Plastic limit $\omega_P$ | Plastic index $I_P$ | Liquidity index $I_L$ |
|---|---|---|---|---|---|---|

| | | | (%) | (%) | | |
|---|---|---|---|---|---|---|
| 1.77 | 1.43 | 21.4 | 29.8 | 17.5 | 12.3 | 0.32 |

A series of ring shear tests were performed to determine the physical properties of the landslide soil after it had been extensively sheared. The saturated soil sample was first consolidated under a normal stress and then it was sheared to a residual state under naturally drained conditions using the shear speed control mode of the ring shear test system. For these tests, normal stresses of 50, 100, 200, 300, and 400 kPa were used to consolidate the soil samples and different shear rates (1, 5, 10, 20 °/min) were employed. Test parameters are listed in Table 2.

**Table 2** Consolidation stresses, shearing rates, and saturations for soil specimens subjected to laboratory ring shear tests.

| Test | Normal stress σ (kPa) | Shear rate α (°/min) | Saturation (%) |
|---|---|---|---|
| 1-1 | 50 | 5 | 100 |
| 1-2 | 100 | 5 | 100 |
| 1-3 | 200 | 5 | 100 |
| 1-4 | 300 | 5 | 100 |
| 1-5 | 400 | 5 | 100 |
| 2-1 | 200 | 1 | 100 |
| 2-2 | 200 | 5 | 100 |
| 2-3 | 200 | 10 | 100 |

Nat. Hazards Earth Syst. Sci. Discuss., https://doi.org/10.5194/nhess-2018-6
Manuscript under review for journal Nat. Hazards Earth Syst. Sci.
Discussion started: 24 January 2018


| | | | |
|---|---|---|---|
| 2-4 | 200 | 20 | 100 |
| 3-1 | 50 | 5 | 0 |
| 4-2 | 100 | 5 | 0 |
| 3-3 | 200 | 5 | 0 |
| 3-4 | 300 | 5 | 0 |
| 3-5 | 400 | 5 | 0 |

### *3.2 Test results and discussion*

(1) Axial stress

Figure 5 shows the relationships between shear stress and angular displacement under a shear rate of 5 °/min and axial stresses of 50, 100, 200, 300, and 400 kPa. At the same shear rate, shear strength increases with increasing axial stress. In the initial shear stages, shear stresses increase rapidly along with shear displacement and reach a peak shear strength. The greater the axial stresses, the larger the shear displacement at peak shear strength. When the axial stress is low (e.g., 50 kPa and 100 kPa), the shear stresses do not change after peak shear strength is reached. When the axial stress is high (e.g., 200 kPa, 300 kPa, or 400 kPa), the shear stresses decrease after peak shear strength but eventually stabilize. This stable strength is the residual shear strength and is the result of strain softening.

Nat. Hazards Earth Syst. Sci. Discuss., https://doi.org/10.5194/nhess-2018-6
Manuscript under review for journal Nat. Hazards Earth Syst. Sci.
Discussion started: 24 January 2018


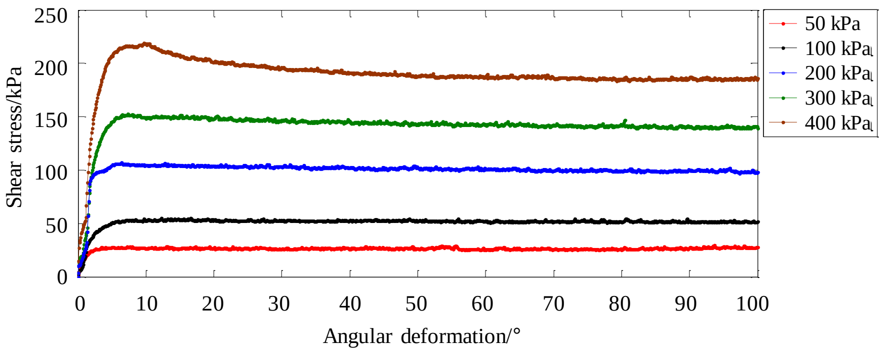


(a) Saturated soil

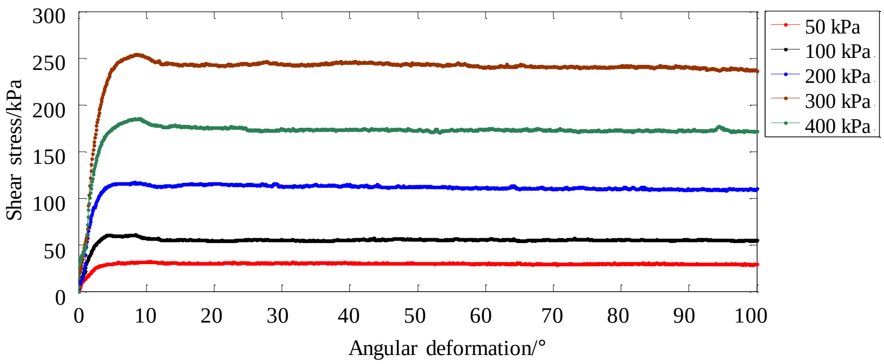


(b) Dry soil

**Fig. 5.** Shear stress–angular displacement curves for the landslide soil at a shear rate of 5°/min and different axial stresses for (a) saturated soil and (b) dry soil.

The residual strength envelope of the soil can be illustrated by plotting the shear stress against axial stress, as shown in Fig. 6.

Nat. Hazards Earth Syst. Sci. Discuss., https://doi.org/10.5194/nhess-2018-6
Manuscript under review for journal Nat. Hazards Earth Syst. Sci.
Discussion started: 24 January 2018


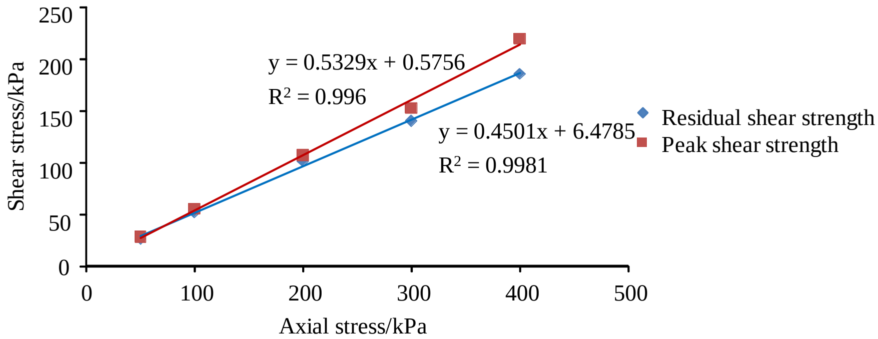


(a) Saturated soil

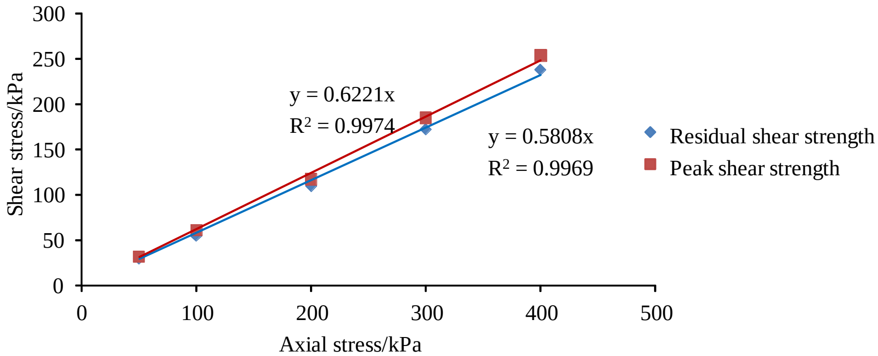


(b) Dry soil

**Fig. 6.** Residual strength envelopes for the landslide soils; (a) saturated soils, (b) dry soils.

Based on Coulomb's equation, the peak and residual shear strengths of the landslide soil were obtained and are listed in Table 3. Because the main trigger for the Dafushan landslide was heavy rain, the residual strength of saturated soil is used for the numerical simulation presented in Section 4 of this paper.

**Table 3** Cohesion and internal friction for landslide soils at peak and residual shear strengths calculated from the Coulomb (Mohr-Coulomb) equation.

Nat. Hazards Earth Syst. Sci. Discuss., https://doi.org/10.5194/nhess-2018-6
Manuscript under review for journal Nat. Hazards Earth Syst. Sci.
Discussion started: 24 January 2018



| Soil | Peak shear strength | | Residual shear strength | |
|---|---|---|---|---|
| | Cohesion $c_r$/kPa | Internal friction angle $\varphi_r$/° | Cohesion $c_r$/kPa | Internal friction angle $\varphi_r$/° |
| Saturated soil | 0.58 | 28.05 | 6.48 | 24.23 |
| Dry soil | 0 | 31.89 | 0 | 30.15 |

(2) Shear rate

Figure 7 shows the relationships between shear stress and angular deformation under a normal stress of 200 kPa at shear rates of 1, 5, 10, and 20 °/min. As the shear rate increases, the residual shear strengths increase slightly but the peak shear strengths show the opposite reaction. However, the angular displacements at peak shear strength increase significantly, as shown in Table 4.

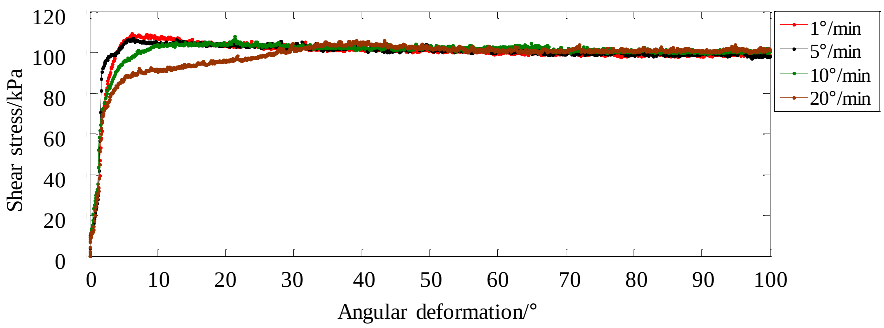


**Fig. 7.** Shear stress–angular displacement curves for saturated landslide soil under 200 kPa axial stress.

**Table 4** Differences in shear strengths and angular displacements for saturated landslide soil at different shearing rates.

| Shearing rate (°/min) | Peak shear strength (kPa) | Residual shear strength (kPa) | Difference between peak and residual shear strength (kPa) | Angular displacement at peak shear strength (°) |
|---|---|---|---|---|
| 1 | 109.10 | 99.35 | 9.75 | 6.264 |
| 5 | 107.00 | 99.52 | 7.48 | 6.444 |
| 10 | 105.00 | 100.55 | 4.45 | 16.992 |
| 20 | 105.80 | 100.99 | 4.81 | 39.168 |

To analyze the relationship between the residual shear strength of the saturated soil and the shear strain rate, the residual shear stress–shear strain rate curve can be drawn (Fig. 8). The formula for calculating the shear strain rate is:

$$\dot{\gamma} = \frac{R\omega}{H} \quad (1)$$

where $\dot{\gamma}$ is the shear strain rate, $R$ is the average radius of the sample, $\omega$ is the angular velocity, $H$ is the sample height.

As shown in Fig. 8, the residual shear strength of the saturated soil as determined by these experiments increases linearly with shear strain rate. This result agrees with the results reported by Li et al. (2013) and Dai et al. (2016). This relationship is similar to the behavior of a viscous fluid and can be expressed by Eq. (2):

$$\tau = \eta\dot{\gamma} + f(\sigma) \quad (2)$$

where $\tau$ is shear stress, $\eta$ is the coefficient of viscosity. The intercept $f(\sigma)$ represents the shear stress when the shear strain rate equals 0.

Nat. Hazards Earth Syst. Sci. Discuss., https://doi.org/10.5194/nhess-2018-6
Manuscript under review for journal Nat. Hazards Earth Syst. Sci.
Discussion started: 24 January 2018


Natural Hazards and Earth System Sciences
Open Access
Discussions

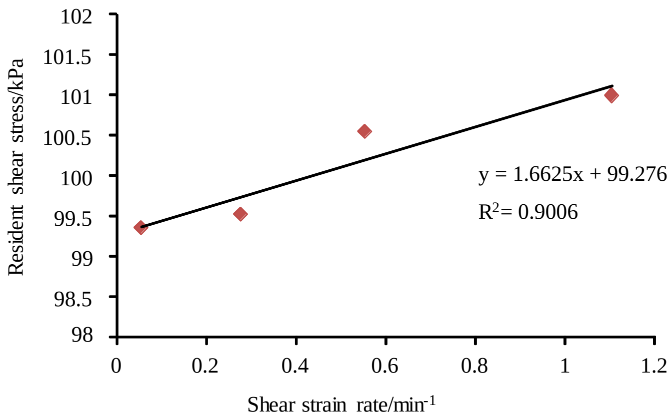


**Fig. 8.** Residual shear stress–shear strain rate curves for the saturated landslide soil.

## 4. SPH-based numerical simulation for landslides

### *4.1 Calculation principles and SPH process methods*

*(1) Basic SPH concepts*

Smoothed particle hydrodynamics is a mesh-free and fully Lagrangian method based on fluid dynamics. In Lagrangian models, the coordinates move with the medium being modeled. The continuous medium is discretized into a series of arbitrarily distributed discrete elements (called particles) and field variables (like energy, velocity, density, or any other variable) for each particle can be calculated in the form of SPH (Dao et al. 2013; Huang and Dai 2014).

The SPH method is built on interpolation theory with two essential approximations. These approximations are smoothing and the particle (Huang et al. 2014). The smoothing approximation, also known as kernel approximation, describes a function in a continuous form as an integral representation. The particle approximation means that the value of a function for a particle can be determined by

Nat. Hazards Earth Syst. Sci. Discuss., https://doi.org/10.5194/nhess-2018-6
Manuscript under review for journal Nat. Hazards Earth Syst. Sci.
Discussion started: 24 January 2018


the average value of all the particles in the support domain. The smoothing and the particle approximations can be expressed, respectively, by the following two equations:

$$\langle f(x) \rangle = \int_{\Omega} f(x') W(x - x', h) dx' \tag{3}$$

$$\langle f(x) \rangle = \sum_{j=1}^{N} m_j \frac{f_j(x)}{\rho_j} W(x - x', h) \tag{4}$$

where the angle brackets represent a kernel approximation, $x$ is the location vector of the particle, $x'$ denotes neighboring particle in the support area, $W$ is the smoothing function, $h$ stands for the smoothing length, $\Omega$ stands for the volume of the integral that contains $x$, $m$ is the mass, and $\rho$ is the density, $N$ is the total number of particles.

*(2) Governing equations*

The Navier–Stokes equations in a computational fluid dynamics framework are used as governing equations in this study. The equations of continuity and motion in the SPH version can be expressed as:

$$\frac{d\rho_i}{dt} = \sum_{j=1}^{N} m_j \left(u_i^{\beta} - u_j^{\beta}\right) \frac{\partial W_{ij}}{\partial x_i^{\beta}} \tag{5}$$

$$\frac{du_i^{\alpha}}{dt} = \sum_{j=1}^{N} m_j \left[ \frac{\sigma_i^{\alpha\beta}}{(\rho_i)^2} + \frac{\sigma_j^{\alpha\beta}}{(\rho_j)^2} \right] \frac{\partial W_{ij}}{\partial x_j^{\beta}} + F_i \tag{6}$$

where $W_{ij}$ represents the smoothing function of particle $I$ calculated at particle $j$, $t$ is time, $u$ denotes the velocity vector, $\sigma$ is the stress tensor, $F$ represents the vector of external force, and $\alpha$ and $\beta$ are the coordinate directions.

*(3) Model for a landslide simulation*

The Bingham model has been proved as one of the most effective models for runout simulation of flowlike landslides (Marr et al. 2002; Moriguchi et al. 2009). In this paper, the Bingham flow model is also adopted as the constitutive model for the Dafushan landslide in this study. The relationship between shear stress and strain rate can be written as:

$$\tau = \eta\dot{\gamma} + \tau_y \, . \tag{7}$$

Equation (8) can be modified by combining it with the Mohr-Coulomb yield criterion to yield (Moriguchi et al. 2009):

$$\tau = \eta\dot{\gamma} + \sigma\tan\varphi + c \tag{8}$$

where $\tau$ denotes the shear stress, $\eta$ and $\tau_y$ represent the Bingham yield viscosity and stress, respectively, $\dot{\gamma}$ is the shear strain rate, $\sigma$ is the pressure, $\varphi$ is the friction angle, and $c$ is the cohesion.

For this study, the concept of equivalent viscosity was adopted to better integrate the Bingham model into the SPH framework. The equivalent viscosity can be expressed as:

$$\eta' = \eta + \tau_y / \dot{\gamma} \, . \tag{9}$$

The maximum value was defined by Uzuoka et al. (1998) as:

$$\eta' = \eta_0 + \frac{\tau_y}{\dot{\gamma}} \qquad \text{when} \quad \eta' < \eta_{\max} \tag{10}$$

$$\eta' = \eta_{\max} \qquad \text{when} \quad \eta' > \eta_{\max} \tag{11}$$

where $\eta_{\max}$ is the maximum value of $\eta'$.

*(4) Procedure for the numerical simulation*

Nat. Hazards Earth Syst. Sci. Discuss., https://doi.org/10.5194/nhess-2018-6
Manuscript under review for journal Nat. Hazards Earth Syst. Sci.
Discussion started: 24 January 2018


A flow chart for the SPH numerical simulation is shown as Fig. 9. Details about how the calculations are carried out can be found in Huang et al. 2014. The accuracy of SPH program in landslide modelling was also fully validated in Huang et al. 2014.

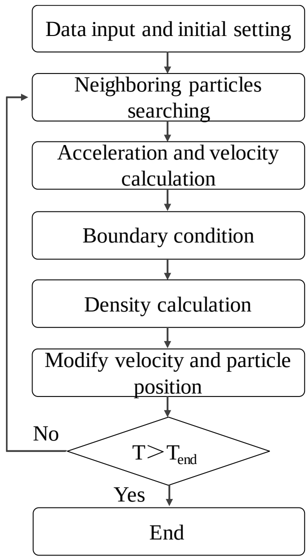


**Fig. 9.** Flow chart for the SPH numerical simulation used in this study.

*4.2 Dafushan landslide SPH simulation and results*

Based on a terrain model derived from an unmanned aerial vehicle and structure-from-motion (Yu et al. 2017), an SPH simulation of the failure process of the Dafushan landslide was conducted. This simulation was used to assess the landslide's effects when failure occur. The numerical model is calculated on the basis of a total of 3,242 particles, 1,537 particles for the slide mass and 1,705 for the fixed boundary. Figure 10 is a longitudinal section of the model slide with the particles in the slide mass shown in red, the boundary particles shown in blue. The diameter of each particle is 0.5 m. The soil particles in the model can be deformed in both the vertical and horizontal directions under gravitational force in the vertical direction.

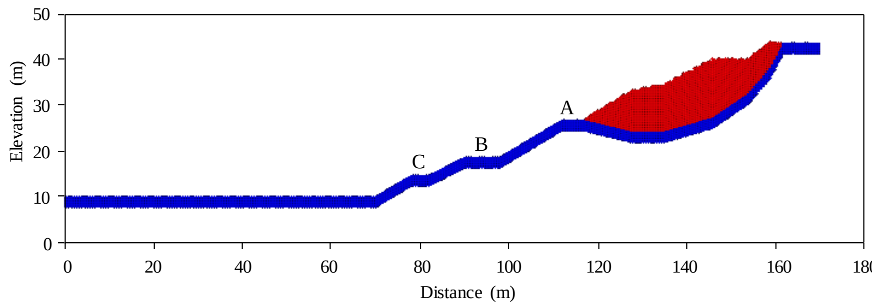


**Fig. 10.** Longitudinal section of the SPH numerical model of the Dafushan landslide. The particles representing the slide mass are shown in red, the particles representing the fixed boundary are shown in blue.

Table 5 lists the parameters used in the SPH simulation of the landslide. The shear strength parameters listed in Table 5, *c* and *φ*, are the values calculated from the ring shear tests (Table 3).

**Table 5** Parameters used in the SPH simulation of the Dafushan landslide.

| | |
|---|---|
| Density $\rho$ (kg/m$^3$) | 1770 |
| Residual cohesion $c$ (kPa) | 6.48 |
| Residual internal friction Angle $\varphi$ (°) | 24.23 |
| Acceleration of gravity $g$ (m/s$^2$) | 9.80 |
| Unit time step $\Delta t$ (s) | 0.003 |
| Time step ($n$) | 40000 |

Figures 11(a)-11(g) show the flow process of Dafushan landslide predicted by the SPH simulation. In Fig. 11, the solid black line represents the bed on which the

Nat. Hazards Earth Syst. Sci. Discuss., https://doi.org/10.5194/nhess-2018-6
Manuscript under review for journal Nat. Hazards Earth Syst. Sci.
Discussion started: 24 January 2018




mass slides, the red dashed line represents the SPH-modeled ground surface. At time t = 0, this red line is the ground surface before slide failure. For times after t = 0, it is the top surface of the flowing mass of soil that constitutes the moving landslide mass as predicted by the SPH simulation results. In the model, the time the failed Dafushan landslide lasts, from initiation to the whole landslide mass coming to rest, is 120 s. The model predicts that the landslide would cut the fire road at t = 12 s and cover the expressway at t = 36 s. When the landslide stops sliding at 120 s, slide material would cover about a 25 m wide swath of ground beyond the foot of the topographic slope.

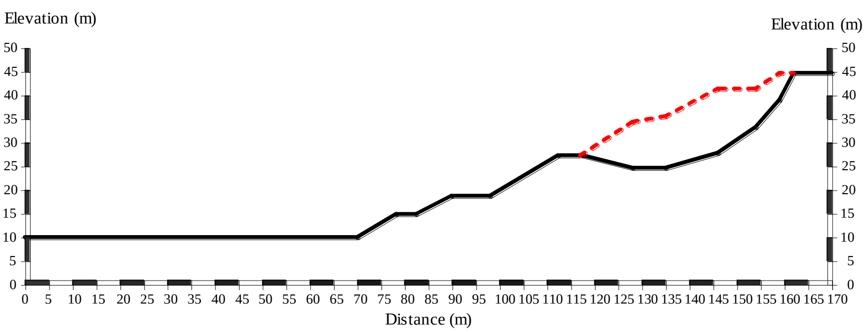


(a) t = 0 s

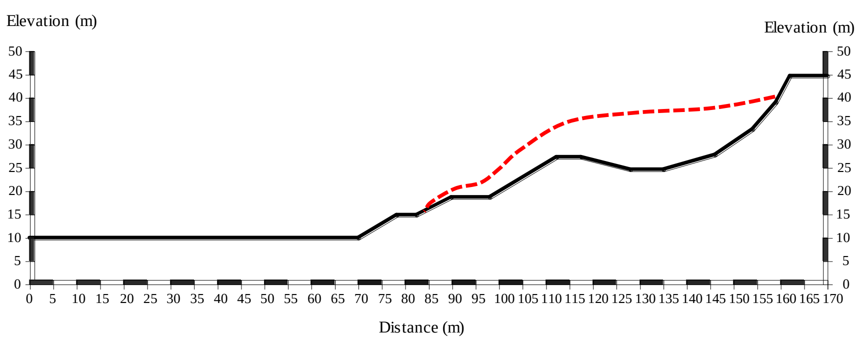


(b) t = 12 s

Nat. Hazards Earth Syst. Sci. Discuss., https://doi.org/10.5194/nhess-2018-6
Manuscript under review for journal Nat. Hazards Earth Syst. Sci.
Discussion started: 24 January 2018

Natural Hazards and Earth System Sciences
Discussions
Open Access

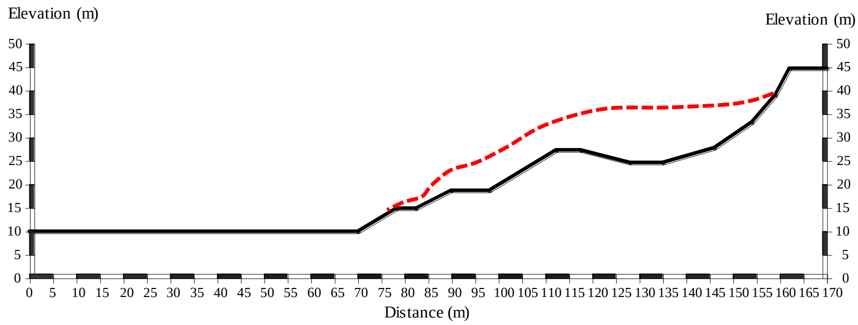


(c) t = 24 s

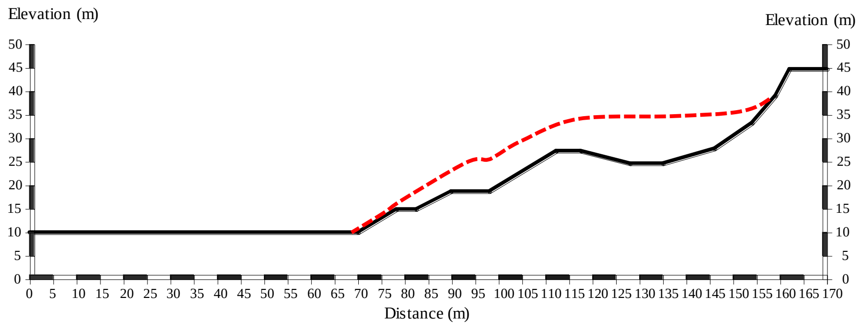


(d) t = 36 s

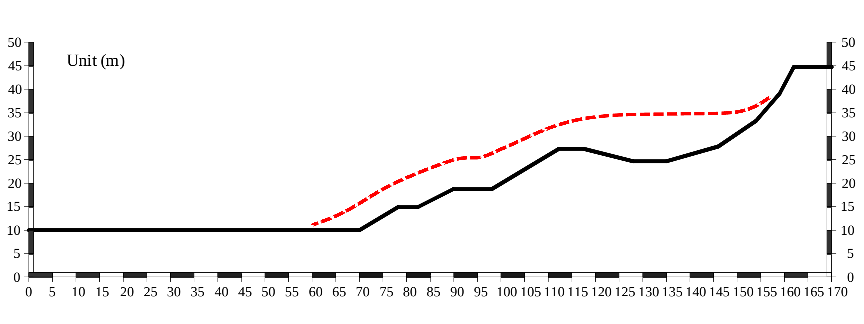

Natural Hazards and Earth System Sciences
Open Access
EGU
Discussions

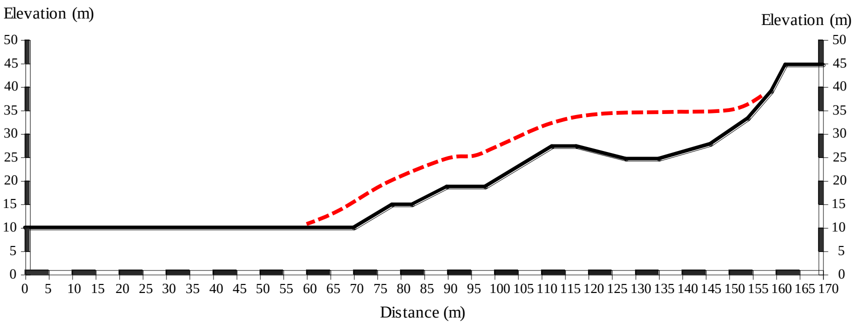


(e) t = 60 s

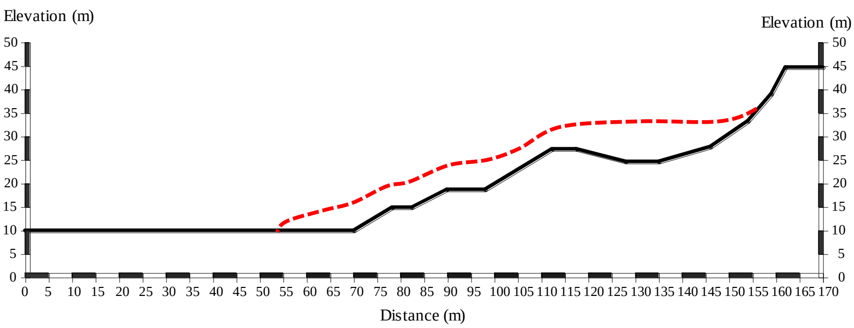


(f) t = 84 s

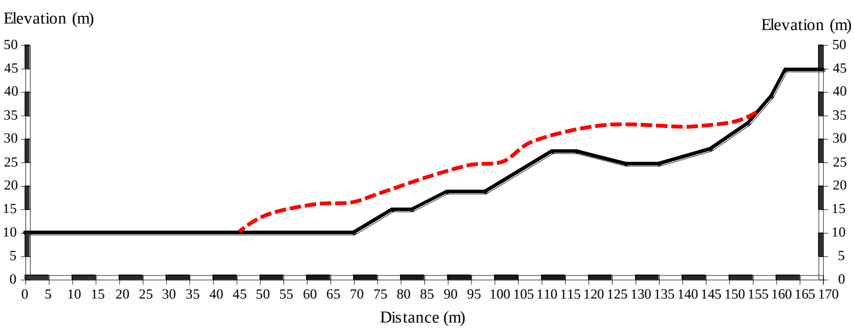


(g) t = 120 s

**Fig. 11.** Longitudinal profiles showing the results of the SPH forecasting model. The panels represent the outline of the Dafushan landslide from the time the slide is

initiated at t = 0 s (panel a) through the slide finally coming to rest at t = 120 s (panel g).

Because this SPH simulation is a Lagrangian method, it can track the velocity and displacement of each particle accurately. The velocity and displacement curves for the front and rear edges of simulated landslide are shown in Figs. 12 and 13. As shown in Fig. 12, the velocity of the front edge increases rapidly after slope failure begins and reaches three velocity peaks as the slide passes the three steps labeled A, B, and C shown in Fig. 10. The speed of the front and the times after initiation that it reaches these three steps are 5.23 m/s at 0.6 s at step A, 6.66 m/s at 9.3 s at step B, and 1.92 m/s at 23.6 s at step C. Unlike the front edge of the landslide, the velocity of the landslide's rear edge shows only a single peak. The maximum speed is 1.40 m/s; this appears 3.8 s after the slide is initiated.

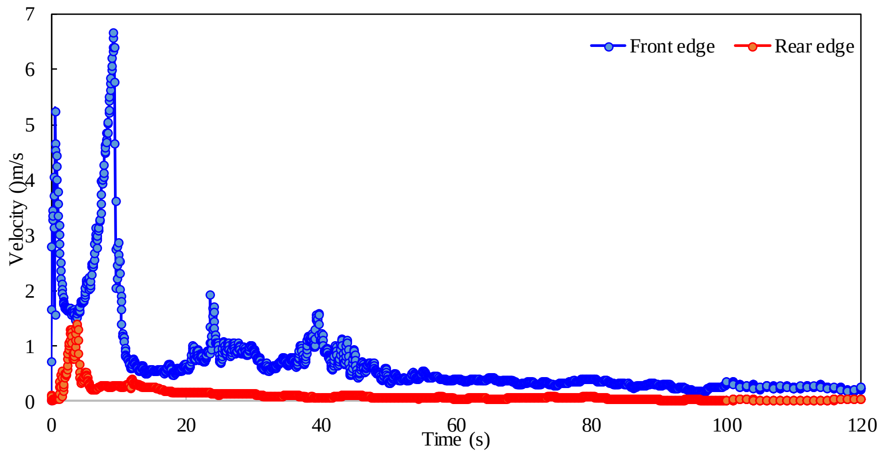


**Fig. 12.** Velocity curve of the front and rear edge of Dafushan landslide as predicted by the SPH model.

Nat. Hazards Earth Syst. Sci. Discuss., https://doi.org/10.5194/nhess-2018-6
Manuscript under review for journal Nat. Hazards Earth Syst. Sci.
Discussion started: 24 January 2018




According to the Fig. 13, the maximum flow distances of the front and rear edge are up to 82 m and 12.3 m, respectively. The front edge of the slide will destroy the fire road about 10–12 s after the slide starts and reach the highway at t = 36 s. Thereafter, the velocity gradually approaches zero as the flow distance increases. The maximum distance the landslide flows is approximately 82 m, and the speed of the flow can be divided into three stages. The flow is fastest from 0–10 s, slower from 10–45 s, and relatively slow from 45–120 s. However, once signs of failure are observed at the Dafushan landslide site, evacuation of personnel and vehicles within about 25 m of the slope should begin immediately.

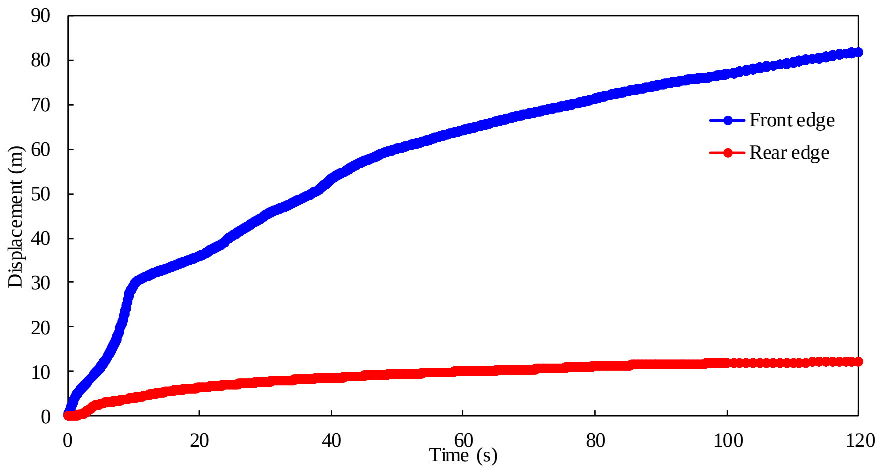


**Fig. 13.** Displacement curve of the front and rear edge of Dafushan landslide as predicted by the SPH model.

## 5. Conclusions

In this study, the SPH method incorporating soil mechanical parameters derived from ring shear tests is used to predict the flow of a potential landslide that could develop on an unstable slope in Guangzhou City, China. This study provides basic information for landside disaster mitigation. The conclusions are:

(1) Under the same shear rate, soil shear strength increases with increasing axial stress. For the conditions used in this study, under high axial stress (> 200 kPa) the soil exhibits strain softening.

(2) During ring shear tests, as the shear rate increases, the residual shear strengths increase slightly but the peak shear strengths decrease as the angular displacements at peak shear strength increase significantly.

(3) A SPH-based numerical simulation of the potential Dafushan landslide conducted to predict the scope of the landslide and track the slide velocity at different times shows that the landslide would cut the fire road at t = 12 s and cover the expressway at t = 36 s. And once signs of failure are observed at the Dafushan landslide site, evacuation of personnel and vehicles within about 25 m of the slope should begin immediately.

**Acknowledgements**

This work was supported by the National Science Fund for Distinguished Young Scholars of China (Grant No. 41625011), the Fundamental Research Funds for National University, China University of Geosciences (Wuhan) (Grant No. CUGL170806), and the National Key Technologies R&D Program of China (Grant No. 2012BAJ11B04).

**References**

[1] ASTM Standard D7608-10 (2010) Standard Test Method for Torsional Ring Shear Test to Determine Drained Fully Softened Shear Strength and Nonlinear Strength Envelope of Cohesive Soils (Using Normally Consolidated Specimen) for Slopes with No Preexisting Shear Surfaces. ASTM International, West Conshonocken, PA

[2] Bui HH, Fukagawa R, Sako K, Ohno S (2008) Lagrangian meshfree particles method (SPH) for large deformation and failure flows of geomaterial using elastic–plastic soil constitutive model. International Journal for Numerical and Analytical Methods in Geomechanics 32(12): 1537–1570

[3] Casagli N, Dapporto S, Ibsen M L, Tofani V, Vannocci P (2006) Analysis of the landslide triggering mechanism during the storm of 20th–21st November 2000, in Northern Tuscany. Landslides 3(1): 13–21

[4] Cascini L, Cuomo S, Pastor M, Sorbino G, Piciullo L (2014) SPH run-out modelling of channelised landslides of the flow type. Geomorphology 214(2): 502–513

[5] Cuomo S, Pastor M, Capobianco V, Cascini L (2016) Modelling the space–time evolution of bed entrainment for flow-like landslides. Engineering Geology 212: 10–20

[6] Dai, Z., Huang, Y., Deng, W., Jiang, F., & Wang, D. (2016) Constitutive flow behavior of a municipal solid waste simulant at post-failure: experimental and numerical investigations. Environmental Earth Sciences 75(11): 1–9

[7] Dao MH, Xu H, Chan ES, Tkalich P (2013) Modelling of tsunami-like wave run-up, breaking and impact on a vertical wall by sph method. Natural Hazards & Earth System Sciences 13(12): 3457–3467

[8] Fukuoka H, Sassa K, Wang G (2007) Influence of shear speed and normal stress on the shear behavior and shear zone structure of granular materials in naturally drained ring shear tests. Landslides 4(1): 63–74

[9] Gattinoni P, Scesi L, Arieni L, Canavesi M (2012) The February 2010 large landslide at Maierato, Vibo Valentia, Southern Italy. Landslides 9(2): 255–261

[10] Hoyos LR, Velosa CL, Puppala AJ (2011) A servo/suction-controlled ring shear apparatus for unsaturated soils: Development, performance, and preliminary results. Geotechnical Testing Journal 34(5): 413–423

[11] Hoyos LR, Velosa CL, Puppala AJ (2014) Residual shear strength of unsaturated soils via suction-controlled ring shear testing. Engineering Geology 172: 1–11

[12] Hu M, Liu MB, Xie MW, Liu GR (2015) Three-dimensional run-out analysis and prediction of flow-like landslides using smoothed particle hydrodynamics. Environmental Earth Sciences 73(4):1629–1640

[13] Huang Y, Dai ZL (2014) Large deformation and failure simulations for geo-disasters using smoothed particle hydrodynamics method. Engineering Geology 168: 86–97

[14] Huang Y, Dai ZL, Zhang WJ (2014) Geo-disaster modeling and analysis: an SPH-based approach. Springer, Heidelberg, pp 184–185

[15] Kimura S, Nakamura S, Vithana SB, Sakai K (2014) Shearing rate effect on residual strength of landslide soils in the slow rate range. Landslides 11(6): 969–979

[16] Li DY, Yin KL, Glade T, Leo C (2017) Effect of over-consolidation and shear rate on the residual strength of soils of silty sand in the Three Gorges Reservoir. Scientific Reports 7(1): 5503

[17] Li YR, Wen BP, Aydin A, Lu NP (2013) Ring shear tests on slip zone soils of three giant landslides in the Three Gorges Project area. Engineering Geology 154(2): 106–115

[18] Liu GR, Liu MB (2003) Smoothed particle hydrodynamics: a meshfree particle method. World Scientific Press, Singapore

[19] Lu CY, Tang CL, Chan YC, Hu JC, Chi CC (2014) Forecasting landslide hazard by the 3D discrete element method: A case study of the unstable slope in the Lushan hot spring district, central Taiwan. Engineering Geology 183: 14–30

[20] Marr J G, Elverhøi A, Harbitz C, Imran J, Harff P (2002) Numerical simulation of mud-rich subaqueous debris flows on the glacially active margins of the Svalbard–Barents Sea. Marine Geology 188(3–4): 351–364

[21] Moriguchi S, Borja R I, Yashima A, Sawada K (2009) Estimating the impact force generated by granular flow on a rigid obstruction. Acta Geotechnica 4(1): 57–71

[22] Okada Y, Ochiai H, Okamoto T, Sassa K, Fukuoka H, Igwe, O (2007) A complex earth slide–earth flow induction by the heavy rainfall in July 2006, Okaya City, Nagano Prefecture, Japan. Landslides 4(2): 197–203

[23] Pastor M, Haddad B, Sorbino G, Cuomo S, Drempetic V (2009) A depth-integrated, coupled SPH model for flow-like landslides and related phenomena. International Journal for Numerical and Analytical Methods in Geomechanics 33(2): 143–172

[24] Tika TE, Hutchinson JN (1999) Ring shear tests on soil from the Vaiont landslide slip surface. Geotechnique 49(1): 59–74.

[25] Tsou CY, Feng ZY, Chigira M (2011) Catastrophic landslide induced by typhoon Morakot, Shiaolin, Taiwan. Geomorphology 127(3): 166–178

[26] Uzuoka R, Yashima A, Kawakami T, Konrod JM (1998) Fluid dynamics based prediction of liquefaction induced lateral spreading. Computers and Geotechnics 22(3–4): 234–282

[27] Van Asch TW, Van Beek LPH, Bogaard TA (2007) Problems in predicting the mobility of slow-moving landslides. Engineering geology 91(1): 46–55

[28] Wang G, Suemine A, Furuya G, Kaibori M, Sassa K (2005) Rainstorm-induced landslides at Kisawa village, Tokushima Prefecture, Japan, August 2004. Landslides 2(3): 235–242

[29] Wen BP, Aydin A, Duzgoren-Aydin NS, Li YR, Chen HY, Xiao SD (2007) Residual strength of slip zones of large landslides in the Three Gorges area, China. Engineering Geology 93(3): 82–98

[30] Wu JH, Lin WK, Hu HT (2017) Assessing the impacts of a large slope failure using 3DEC: The Chiu-fen-erh-shan residual slope. Computers & Geotechnics 88:32–45.

[31] Yerro A, Alonso EE, Pinyol NM (2016) Run-out of landslides in brittle soils. Computers & Geotechnics 80:427–439

[32] Yu M, Huang Y, Zhou JM, Mao LY (2017) Modeling of landslide topography based on micro-unmanned aerial vehicle photography and structure-from-motion. Environmental Earth Sciences 76(15): 520

[33] Zhang M, Yin Y, Hu R, WS, Zhang Y (2011) Ring shear test for transform mechanism of slide–debris flow. Engineering Geology 118(3): 55–62

[34] Žic E, Arbanas Ž, Bićanić N, Ožanić N (2015) A model of mudflow propagation downstream from the grohovo landslide near the city of rijeka (croatia). Natural Hazards & Earth System Sciences 15(2): 293–313